

# Total cross section of $^{14}\text{N}+n$ from 0.1 to 12 MeV

R.J. deBoer,<sup>1,\*</sup> R. Arquette,<sup>2</sup> D. Bemmerer,<sup>3</sup> A. Best,<sup>4,5</sup> R. Beyer,<sup>3</sup> A. Boeltzig,<sup>3</sup> G. Clarke,<sup>2</sup> J. Görres,<sup>1</sup> T. Hensel,<sup>3</sup> A.R. Junghans,<sup>3,†</sup> M. Matney,<sup>1</sup> S.E. Müller,<sup>3</sup> D. Rapagnani,<sup>4,5</sup> A. Roberts,<sup>2</sup> K. Römer,<sup>3</sup> S. Turkat,<sup>6</sup> K. Schmidt,<sup>3</sup> J. Skowronski,<sup>7,8</sup> A. Wagner,<sup>3</sup> M. Wiescher,<sup>1</sup> and A. Yadav<sup>3</sup>

<sup>1</sup>*Department of Physics and Astronomy, University of Notre Dame, Notre Dame, Indiana 46556 USA*

<sup>2</sup>*Department of Physics, University of Colorado Denver, Denver, Colorado 80204 USA*

<sup>3</sup>*Helmholtz-Zentrum Dresden-Rossendorf, 01328 Dresden, Germany*

<sup>4</sup>*Università degli Studi di Napoli “Federico II”, Dipartimento di Fisica “E. Pancini”, Via Cintia, 80126 Napoli, Italy*

<sup>5</sup>*INFN - Sezione di Napoli, Via Cintia, 80126 Napoli, Italy*

<sup>6</sup>*Institut für Kern- und Teilchenphysik, Technische Universität Dresden, 01062 Dresden, Germany*

<sup>7</sup>*Dipartimento di Fisica, Università degli Studi di Padova, 35131 Padova, Italy*

<sup>8</sup>*INFN, Sezione di Padova, 35131 Padova, Italy*

(Dated: May 9, 2025)

The reaction  $^{14}\text{N}(n,p)^{14}\text{C}$  is one of the main neutron poisons during *s*-process nucleosynthesis. In addition, the reaction provides insight into the yields of atmospheric nuclear weapon testing. Because of their high level of sensitivity, total neutron cross sections provide a great deal of constraint on the modeling of reaction cross sections through the *R*-matrix analyses used for nuclear data evaluations. Yet for  $^{14}\text{N}+n$ , only one high sensitivity measurement is available and it lacks detailed information about its experimental conditions and uncertainties. With these motivations in mind, a new measurement of the  $^{14}\text{N}+n$  total cross section has been performed at the nELBE facility. The cross sections were found to be in good agreement with previous data over much of the energy range with the key exception of the lowest energy resonance at a neutron energy of 433 keV.

## I. INTRODUCTION

The  $^{14}\text{N}(n,p)^{14}\text{C}$  reaction is a key nuclear physics ingredient in understanding neutron production for the main *s*-process (see, e.g., Wallner *et al.* [1]). The high cross section combined with the large amount of  $^{14}\text{N}$  present in the main *s*-process environment, means that it acts as an efficient neutron poison. The lowest energy strong resonance in the  $^{14}\text{N}(n,p)^{14}\text{C}$  reaction is a relatively narrow one at  $E_{\text{c.m.}} = 458$  keV ( $J^\pi = 1/2^-$ ,  $\Gamma \approx 8$  keV). For this reason, the cross section over the low-energy region is mainly non-resonant, made up of contributions from the high-energy tails of subthreshold states and the low-energy tails of broad higher-energy resonances. At low energies ( $61 \text{ meV} < E_n < 34.6 \text{ keV}$ ), the cross section has been carefully mapped by Koehler and O’Brien [2] who found that it was dominated by the tail contributions of subthreshold states that produce a low-energy cross section that rapidly increases towards lower energy. Several additional measurements have been made [1–5] that sample only a few energies but cover an energy range from  $20 \text{ keV} \lesssim E_n \lesssim 178 \text{ keV}$ . The measurements over this range are in reasonably good agreement, except for those of Brehm *et al.* [3], which are about a factor of two lower in cross section. There is then a gap in the experimental data between the measurements of Wallner *et al.* [1] and Morgan [6] ( $178 \text{ keV} < E_n < 464 \text{ keV}$ ). Johnson and Barschall [7] reportedly performed measurements over this region, but

the data lack uncertainties. Recently Torres-Sánchez *et al.* [8] have remeasured over this energy range, but to compare their yield data with cross section calculations large resolution corrections need to be applied, introducing additional uncertainties. As there are many broad resonances at higher energies, whose low energy tails can conceivably contribute to the cross section over this region, interpolation over this energy region remains uncertain.

This was recently demonstrated by Wallner *et al.* [1] in their comparison between their data and the JEFF-3.2 evaluation. It should be noted that the JEFF-3.2 evaluation [9] of  $^{14}\text{N}+n$  [10] is the same as that of ENDF/B-VI.3 [11] and that the evaluation at low energy is based on the *R*-matrix analysis of Hale *et al.* [12] that has not been re-evaluated as of ENDF/B-VIII.0 [13], but a revised evaluation of  $n+^{14}\text{N}$  reactions is currently underway [14–16].

In addition,  $^{14}\text{N}+n$  reactions are of interest for simulating neutron transport through a variety of materials. For example, the  $^{14}\text{N}(n,p)^{14}\text{C}$  reaction is the main source of  $^{14}\text{C}$  in the earth’s atmosphere. Neutrons for the reaction are either naturally produced from cosmic rays interacting with the atmosphere or were produced through above-ground nuclear weapons testing which significantly has influenced the radio-carbon method of age determination [17]. Using the  $^{14}\text{N}(n,p)^{14}\text{C}$  cross section and sampling the increased levels of  $^{14}\text{C}$  in the atmosphere, information about a nuclear explosion can be inferred (see, e.g., Burr [18]).

There have been several studies of reactions that populate the  $^{15}\text{N}$  system over the excitation energy range of interest. These reactions include not only  $^{14}\text{N}+n$ , but also  $^{14}\text{C}+p$  and  $^{11}\text{B}+\alpha$ , partly because of the close prox-

\* rdeboer1@nd.edu

† a.junghans@hzdr.de

imity of their separation energies:  $S_p = 10.207$  MeV,  $S_n = 10.833$  MeV, and  $Q_\alpha = -10.991$  MeV. For the  $^{11}\text{B}(\alpha, n)^{14}\text{N}$  reaction, there have been only a few studies [19–21], where that of Wang *et al.* [21] was the most comprehensive. Studies of the  $^{11}\text{B}(\alpha, p)^{14}\text{C}$  reaction have been made by Refs. [21–23] and the  $^{11}\text{B}(\alpha, \alpha)^{11}\text{B}$  reaction by Refs. [24, 25]. Studies of  $^{14}\text{C}+p$  reactions include measurements of  $^{14}\text{C}(p, p)^{14}\text{C}$  [26, 27],  $^{14}\text{C}(p, n)^{14}\text{N}$  [19, 21, 28–31], and  $^{14}\text{C}(p, \gamma)^{15}\text{N}$  [27, 28, 32]. Finally, studies of neutron induced reactions on  $^{14}\text{N}$  include  $^{14}\text{N}(n, n)^{14}\text{N}$  [33],  $^{14}\text{N}(n, p)^{14}\text{C}$  [6–8, 31, 34] (fast neutrons),  $^{14}\text{N}(n, \alpha)^{11}\text{B}$  [6, 7, 34], and  $^{14}\text{N}(n, \text{total})$  [10, 35, 36]. Of particular note for this work is the high resolution and comprehensive measurement of the  $^{14}\text{N}(n, \text{total})$  cross section by Harvey *et al.* [10] at Oak Ridge National Laboratory.

## II. EXPERIMENTAL SETUP

Helmholtz-Zentrum Dresden - Rossendorf (HZDR) operates the first photo-neutron source (nELBE) at a superconducting electron accelerator dedicated to measurements in the fast neutron range [37, 38]. The floor plan of the facility is shown in Fig. 1. The superconducting electron accelerator (ELBE) accelerates electrons to a kinetic energy of typically 30 MeV in continuous-wave mode. The micro-pulse repetition rate is reduced to 101 kHz with a reduced bunch charge of approximately 10 pC to avoid an excessive bremsstrahlung intensity and neutron pulse overlap in time-of-flight measurements. The electron micro pulses have a duration of only 5–10 ps and thus allow for an excellent time resolution. A compact liquid-lead circuit is utilized as a neutron-producing target. The neutron radiator consists of a Mo-tube with a rhombic cross-section and a diameter of 11 mm through which liquid lead is pumped. The neutrons leave the neutron-producing target almost isotropically, whereas the angular distributions of electrons and bremsstrahlung are strongly forward-peaked. The collimator axis is located at an angle of  $100^\circ$  with respect to the electron beam direction. A lead absorber of 5 cm thickness mounted halfway between the neutron producing target and the collimator entrance is used to suppress the bremsstrahlung intensity (gamma flash). The target samples are mounted in a target ladder in front of the collimator entrance at a distance of 1 m from the neutron-producing target. The properties of the collimator and the neutron beam at the experimental area have been optimized in order to maintain the correlation of time-of-flight and neutron energy [37]. The collimator has a length of 2.5 m and contains three inserts of lead and borated polyethylene that are mounted inside a precision steel tube. All walls, ceiling and floor in the time-of-flight experimental hall are at least 3 m away from the neutron beam axis to help reduce the room return neutrons.

The neutrons were detected with a fast EJ-228 plastic scintillator bar with dimensions  $200 \times 20 \times 5$  mm<sup>3</sup> read out

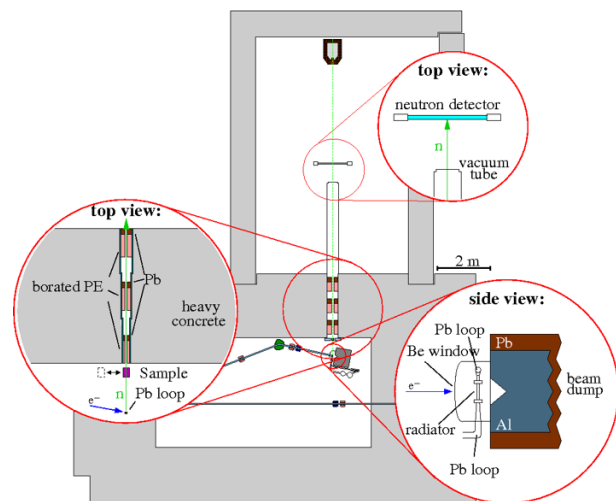


FIG. 1. Floor plan of the neutron time-of-flight facility nELBE at HZDR. The neutrons are produced by the electron beam hitting a liquid lead circuit as neutron producing target, see inset on the lower right. The neutron beam is shaped by a collimator and guided to the neutron time-of-flight hall, see inset on the left. The detection setup is located in the time-of-flight hall, see upper inset. For neutron transmission experiments a plastic scintillator with a low threshold for recoil proton signals ( $E_n > 10$  keV) is used. The transmission samples are located in a movable absorber ladder in the front of the collimator.

on both ends by high-gain PMTs Hamamatsu R2059-01. By a narrow time-coincidence window on both PMT signals, a detection threshold of about 10 keV neutron energy has been obtained [39]. The flight path  $L$  was determined to be 868.2(3) cm long including an offset of 0.5 cm based on a comparison of measured resonance energies from transmission of N, O, Ne, Ar, and C at nELBE in comparison with the corresponding energies given in the Atlas of Neutron Resonances ref.[40]. The neutron count rate was typically 700 - 1000 per second while the bremsstrahlung pulses detected had a count rate of a 10000 - 15000 per second. The transmission measurement was made with a gaseous nitrogen sample using high-pressure gas cells made from stainless steel tubing with flat end-caps of 3 mm wall thickness. A cross section cut of the gas cell is shown in Fig. 2. To cancel the transmission factor through the end caps a second identical evacuated cell was used in the “target out of beam” measurements.

The target areal density was determined by measuring the temperature and pressure during and after the filling procedure of the gas target using a high-precision pressure transducer with an absolute accuracy of 0.125 bar. The nitrogen gas with natural isotopic composition was supplied from a new high-purity bottle with a purity of 99.999%. The fluid equation of state used to convert the measured pressure and temperature to atomic density was taken from the National Institute of Standards and Technology (NIST) data base [41]. The nitrogen

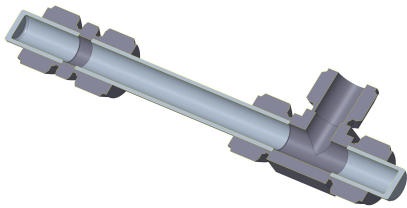


FIG. 2. Cross section cut of a high pressure gas cell used for nitrogen transmission measurement. The cell is made from stainless steel with cylindrical end-caps having a wall thickness of 3 mm using standard Swagelock components. The maximum pressure is up to 200 bar. The length of the gas volume is 393 mm. The tube is made from 30×3 mm stainless steel. Not shown in the rendering are the valve and pressure gauge connected on the open ended flange.

atomic areal density of the sample was determined to be  $nl = 0.19736(24)$  atoms/barn at 102.00 bar absolute pressure and a temperature of 20.4 °C. The time-of-flight of the transmitted neutrons was measured in list mode with the real-time data acquisition software package MBS (Multi-Branch-System) [42] developed at Gesellschaft für Schwerionenforschung (GSI), Darmstadt. The data acquisition setup consists of a single Versa Module Euro-card (VME)/ Nuclear Instrument Module (NIM) crate with a CES RIO4 front-end processor using the real-time operating system Lynx OS. The photo-multiplier tube (PMT) signals and the accelerator frequency are fed into a CAEN V1290A multi-hit multi-event time-to-digital converter (TDC) with (1/40.96) ns least significant bit (LSB). This TDC is operated in trigger matching mode using a programmable time window with 13  $\mu$ s width. The time-of-flight spectrum is determined from the coincident time sum of both PMT signals relative to the accelerator frequency. A software condition is set on the time-difference of the two PMT signals to select events from the center of the beam spot on the scintillator and to reduce the detection of double hits. A dead time of 4  $\mu$ s was inserted after each coincidence hit to efficiently suppress PMT afterpulses that mainly arise from the gamma-flash. The dead time was measured per event and used to generate a time-of-flight dependent live-time factor discussed in the next section. Typical time-of-flight spectra are shown in Fig. 3.

### III. DATA ANALYSIS

The neutron transmission  $T_{exp}(t_i)$  is determined from the ratio of the background and dead time corrected

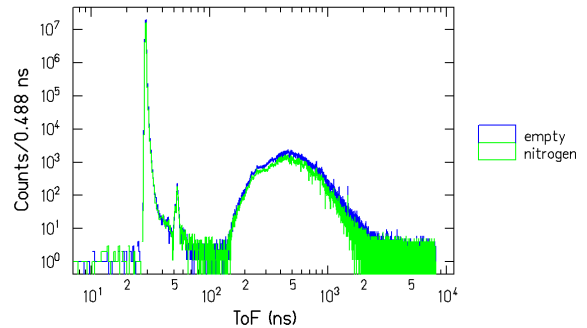


FIG. 3. Time-of-flight spectra after dead-time correction with the empty gas cell and the nitrogen filled gas cell (102 bar) in the beam. The gamma-flash due to bremsstrahlung is centered at 28.945 ns with a width (FWHM) of 0.47 ns. The smaller peak to the right is due to radiation back scattered from the beam dump and rear wall. The neutron time-of-flight ranges extends from 150 ns to 2.5  $\mu$ s. Random background is not subtracted in this plot.

count rates with nitrogen sample in the beam (in) to the empty gas cell (out) as a function of neutron time-of-flight channel  $t_i$ :

$$T_{exp}(t_i) = \frac{\sum_k (N_{in,k}(t_i) - B_{in,k}(t_i)) f_{in,k}}{\sum_k t_{real,in,k}} \cdot \frac{\sum_k t_{real,out,k}}{\sum_k (N_{out,k}(t_i) - B_{out,k}(t_i)) f_{out,k}} \quad (1)$$

where  $N_{in/out}(t_i)$  and  $B_{in/out}(t_i)$  are the dead time corrected numbers of detected events and level of background events in each time-of-flight channel  $i$  with and without the nitrogen target in the beam. The real times for each run  $k$  with target in/out are denoted by  $t_{real,in,k}$  and  $t_{real,out,k}$ . The dead-time correction is time-of-flight dependent, as explained in Beyer *et al.* [43]. The biggest part is caused by the gamma flash while only a smaller effect is due to the later arriving neutrons. The live time factors as a function of time-of-flight are shown in Fig. 4. The absolute time-of-flight scale was determined for each run with the measured absolute gamma-flash peak position from the TDC, the nominal flight path  $L$  and the speed of light.

The transmission experiment was done by periodically moving the nitrogen sample and empty gas cell in and out of the beam with counting times adapted to maximize the statistics. Typical counting times for each setting were 10 min empty and 20 min with nitrogen for a total beam time of 156 hours. Listmode data were recorded in separate runs of about 2-4 hours. The spectrum average neutron and gamma-count rates for each run are plotted in Fig. 5 to illustrate the average beam stability in the measurement. The relative beam stability (standard deviation / mean value) of the average count rates of the separate runs amounts to 0.05.

The transmission was calculated using the sum of all

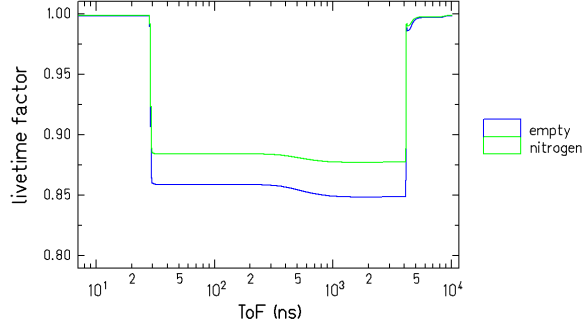


FIG. 4. The time-of-flight dependent live time factors for the measurements with empty gas cell and the gas cell containing nitrogen are shown on a logarithmic time scale. The nearly rectangular shape is due to the 4  $\mu$ s long induced dead time after each trigger signal to suppress PMT after pulses, which are mostly due to the gamma flash signals.

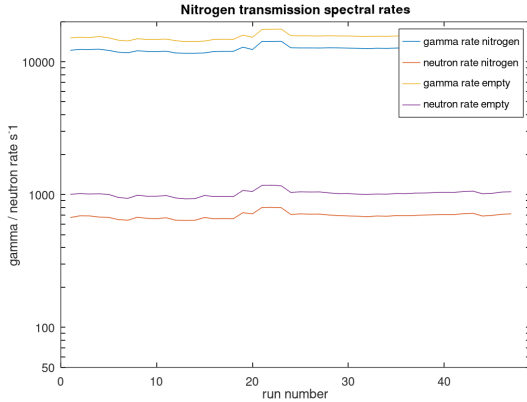


FIG. 5. The spectrum total count rates for the bremsstrahlung and neutron events are shown for subsets of the data (runs) lasting 2-4 hours typically including several target-in and out sample changes.

these runs  $k$  where no beam intensity fluctuation or failure occurred in the “sample in” and “empty gas cell” settings. The factors  $f_{in,k}$  and  $f_{out,k}$  are normalization factors to correct for the remaining fluctuations in the neutron source intensity:

$$f_{out,k} = \frac{t_{real,out,k}}{\sum_i (N_{out,k}(t_i) - B_{out,k}(t_i))} \quad (2)$$

$$f_{in,k} = \langle T \rangle \frac{t_{real,in,k}}{\sum_i (N_{in,k}(t_i) - B_{in,k}(t_i))} \quad (3)$$

The neutron count rate for each run  $k$  with target out of the beam summed over the full neutron time-of-flight range  $i$  is used as a neutron source intensity monitor in Eq. (2). For the “target in” settings, the neutron source intensity monitor is approximated with the target-in count rate divided by the mean integral transmission

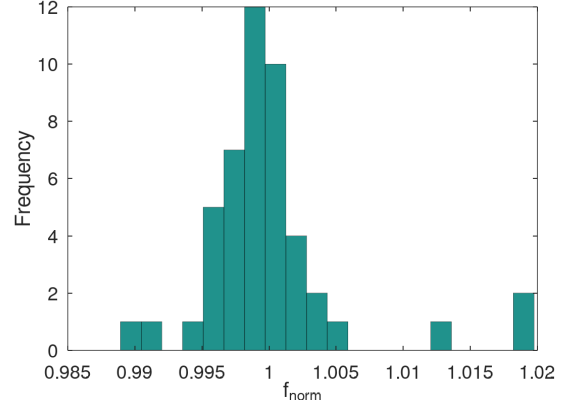


FIG. 6. The distribution of  $f_{in,k}/f_{out,k}$ , see Eqs. (2) and (3), is shown for subsets of the data (runs) lasting 2-4 hours typically including several target-in and out sample changes.

factor  $\langle T \rangle$  over the full neutron time-of-flight range  $i$  of the full experiment including all runs  $k$ . The distribution of the normalization factors  $f_{in,k}/f_{out,k}$ , see Eqs. (2) and (3), is shown in Fig.6. The mean value is one by definition and the standard deviation is 0.005.

From the measured transmission as a function of time-of-flight  $T_{exp}(E_n(t_i))$ , an effective neutron total cross section  $\langle \sigma_{tot}(E_n) \rangle$  can be determined:

$$\langle \sigma_{tot}(E_n) \rangle = -\frac{1}{nl} \ln T_{exp} \quad (4)$$

where  $nl$  is the atomic areal density of the target sample.

To determine the neutron transmission and the total cross section from the measured time-of-flight distribution with a relative accuracy of a few percent, several corrections need to be considered:

1. Correction for a time-of-flight dependent dead time,
2. Subtraction of a random background in the time-of-flight spectra,
3. Correction for fluctuations of the neutron-beam intensity,
4. Correction for in-scattering of neutrons,
5. Correction for resonant self-shielding in thick transmission samples.

Random background and dead-time corrections are important at low and high neutron energy, where the neutron source intensity is already decreasing. In this experiment a low beam intensity and a very compact neutron-producing target without any materials that would slow down neutrons were used. There is no neutron moderator in the target setup and the amount of in-beam gamma-rays from neutron capture is negligible. The random background can be described by a constant value in time-of-flight spectrum. It is mostly dominated by random coincidences due to ambient natural radioactivity,

whereas the room return background of neutrons is relatively low [44]. The determination of the background levels  $B_{in/out}$  is done by calculating the mean bin content in the time-of-flight ranges before the  $\gamma$ -flash and between 4.68 to 7  $\mu$ s. In the time-of-flight region around 150 ns, before the first fast neutrons arrive, the background level is higher than estimated from the mean bin content between 4.68 to 7  $\mu$ s. This background tail is due to insufficient suppression of PMT after-pulses mostly from the gamma-flash. Due to the low background-to-total ratio, it has been neglected in the transmission determination [43]. The background-to-total ratio is shown in Fig. 7. As the background is taken as a constant value from outside of the neutron time-of-flight range, the spectra show peaks and dips which are related to the pure source spectrum, which contains known peaks from near-threshold photo neutron production in lead and from the resonant structure of the nitrogen and other layers of matter in the beam. In the neutron energy range below 200 keV the neutron intensity from the source decreases and uncertainties in the background shape get large enough to influence the transmission measurement. The uncertainties of the transmission measurement and total cross-section determination have already been discussed in Hannaske *et al.* [44] and Beyer *et al.* [43]. The important uncertainties will be briefly revisited here. The fluctuations of the neutron-beam intensity were measured during the sample cycling and found to have a small influence. From transmission values determined from subsets of the data, a fluctuation of less than 0.5% was found and included in the total systematic uncertainty. In-scattering of neutrons was minimized by the geometry of the setup: The collimator strongly limits the solid angle under which neutrons can be registered and only neutrons passing through the full length of the sample can hit the detector. The probability for multiple in-scattering of fast neutrons has been found to be less than 0.1% [44].

In Fig. 8 the uncertainty budget of the total cross section is shown for the nitrogen sample measurements. The plot looks similar for the empty target measurements. To quantify the contribution of each parameter  $X \in \{N_{in}, \alpha_{in}, BG_{in}\}$  used to determine the total cross section  $\sigma$  the quantity  $\frac{\partial \sigma}{\partial X} \frac{\Delta X}{\sigma}$  was calculated by differentiating Eq. (1). These quantities are plotted for a time-of-flight bin size of 1 ns. It is visible that the uncertainty of the background level due to counting statistics ( $BG_{in/out,stat}$ ) is negligible for the overall uncertainty due to statistical effects  $\frac{\Delta \sigma}{\sigma}(\text{stat.})$ . The contribution of the uncertainty of the background level due to the inclusion of the energy-dependent uncertainty ( $BG_{in/out,sys}$ ) to the overall uncertainty due to systematic effects  $\frac{\Delta \sigma}{\sigma}(\text{sys.})$  becomes noticeable at the upper and lower ends of the neutron energy spectrum available at nELBE. Nevertheless, over the complete energy range, the uncertainty of the flux normalization factor  $f_{norm}$  is dominating the systematic uncertainty. The uncertainties of the samples areal density ( $nl$ ) and the dead time correction factor ( $\alpha$ ) are less important. In total,  $\frac{\Delta \sigma}{\sigma}(\text{sys.})$  sums up to

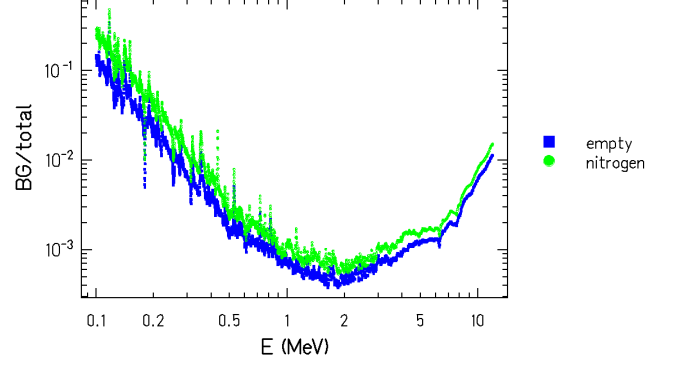


FIG. 7. The background to total counts ratios are shown for the full data set of the transmission measurement. The green data points (circles) were measured with the nitrogen sample in the beam, the blue data points (squares) with the empty gas cell. The statistical uncertainties have not been plotted to improve the visibility of the structures in the spectra.

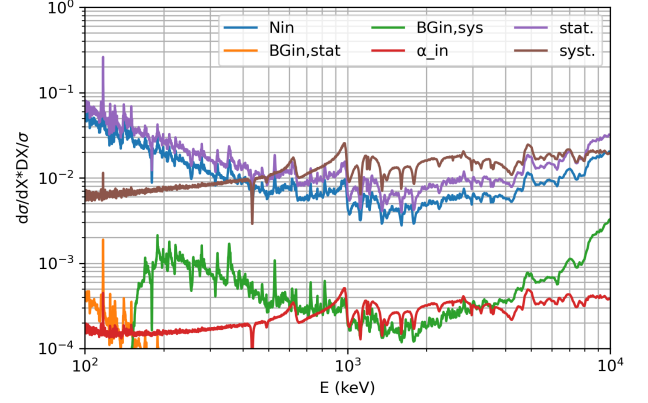


FIG. 8. The uncertainty budget of the measured total cross section of nitrogen. The relative contribution of each parameter  $X \in \{N_{in}, \alpha_{in}, BG_{in}\}$  to the uncertainty of the total cross section  $\sigma$  due to statistical (stat.) and systematic (sys.) effects is shown for a time binning of 1 ns. The total statistical (purple) and systematic (brown) uncertainty also contain the contributions from the target out data.

about 1.5%.

The measured neutron transmission of nitrogen is shown in Fig. 9 and Fig. 10 compared to a calculated transmission curve based on the evaluated cross section from ENSDF/B VIII.0. The measured transmission extends through the fast neutron energy range from about 0.1 to 12 MeV. The nitrogen thickness was chosen in order not to saturate the first resonance at 433 keV neutron kinetic energy. The energy resolution of the time-of-flight measurement determines how well the resonant structure of the underlying total cross section can be observed.

The resolution function of nELBE is modeled as a



Gaussian function

$$R(E - E') = \frac{1}{\Delta E \sqrt{2\pi}} \exp\left(-\frac{1}{2} \frac{(E - E')^2}{(\Delta E)^2}\right) \quad (5)$$

with the RMS width  $\Delta E$ , which consists of the time resolution of the plastic scintillator  $\Delta t$  used for detecting the transmitted neutrons and the standard deviation of the nominal flight length  $\Delta L$  due to the combined thickness of the neutron producing target and the plastic scintillator  $\Delta L$

$$\frac{\Delta E}{E} = (\gamma + 1) \frac{\Delta v}{v} \quad (6)$$

$$\frac{\Delta v}{v} = \sqrt{\left(\frac{\Delta t}{t}\right)^2 + \left(\frac{\Delta L}{L}\right)^2} \quad (7)$$

where  $\gamma$  is the Lorentz parameter for a neutron with kinetic energy  $E$  and velocity  $v$ . The time resolution of the plastic scintillator was determined experimentally from the measured width of the bremsstrahlung peak. As the electron beam pulse length is only 5-10 ps, the measured width corresponds closely to the time resolution ( $\Delta t = 0.20$  ns, 1 std. dev.). The width of the neutron producing target (11 mm) and the plastic scintillator (5 mm) give  $\Delta L = \sqrt{((1.1 \text{ cm})^2 + (0.5 \text{ cm})^2)/12} = 0.35$  cm, 1 std. dev, where division by  $\sqrt{12}$  converts the FWHM of the rectangular flight path distribution to the standard deviation of an equivalent Gaussian. The transmission curve including the experimental resolution with the ENDF/B-VIII.0 evaluated cross section has been calculated by numerical integration of

$$T(E) = \int R(E - E') \exp(-nl\sigma_{\text{ENDF}}(E')) dE'. \quad (8)$$

#### IV. R-MATRIX ANALYSIS

$R$ -matrix calculations were performed using the code **AZURE2** [45], representing a continued analysis of the  $^{15}\text{N}$  system as presented previously in deBoer *et al.* [46] and Borgwardt *et al.* [47]. The  $R$ -matrix calculations utilize the alternative parameterization of Brune [48] so that observable resonance parameters can be used directly as inputs for the  $R$ -matrix calculations instead of formal ones [49]. It also eliminates the need for boundary condition parameters, leaving the channel radius as the sole model parameter. The typical simplification has been made that the same channel radius is used for all channels of a given particle partition. The  $\alpha$ -particle, proton and neutron channel radii were 5.5, 5.0, and 4.0 fm, respectively.

Although the present total neutron cross section measurements extend up to  $E_n \approx 12.0$  MeV, the analysis concentrates on the energy region below  $E_n < 1$  MeV

in order to both simplify the  $R$ -matrix analysis and because the focus is to investigate the properties of the  $E_n = 433$  keV resonance observed in the total neutron cross section data. Over this energy range, there are only three particle partitions that are energetically accessible:  $n+^{14}\text{N}$ ,  $p+^{14}\text{C}$ , and  $\alpha+^{11}\text{B}$ , all only accessing the ground state. Since, for several resonances, the corresponding compound nucleus levels have proton and  $\alpha$ -particle partial widths with similar strength compared to the neutron partial width, the inclusion of these other partitions are needed to reproduce the total neutron cross section. To constrain the branchings of these partial widths in the fit, representative data sets [2, 6, 26, 47] from these other reaction channels are also included to improve the fidelity of the fit. The fit is shown in Fig. 12.

To estimate uncertainties for the  $R$ -matrix fit, the Bayesian  $R$ -matrix Inference Code Kit (**BRICK**) [50] was utilized. **BRICK** is a Python package that serves as a mediator between the **AZURE2**  $R$ -matrix code and the MCMC sampling software **emcee** [51]. Uncertainties for the level parameters as well as those for the cross sections that were fit were extracted. The Bayesian uncertainty analysis included the systematic uncertainties of each data set as a Gaussian prior. More information can be found in the Supplemental Material [52].

#### V. DISCUSSION

When the resolution function for the present measurements is applied to the  $R$ -matrix cross section, there is good agreement between the data of this work and those of Harvey *et al.* [10] over nearly the entire overlapping energy range. The comparison of the experimental total cross section measured in this work with Harvey *et al.* [10] in Fig. 11 shows already this good agreement. The exceptions are in the shapes of some of the narrow resonances (1184 keV), where the most discernible differences are in the first resonance at  $E_n = 433$  keV. This resonance was first observed in total cross section measurements in 1951 by Johnson *et al.* [36], but its level properties proved difficult to constrain due to its narrow width. In both the early measurements of Johnson *et al.* [36] ( $E_n = 433$  keV) and Hinchey *et al.* [35] ( $E_n = 430$  keV,  $\Gamma = 3.5$  keV), the total width was reported to be similar to the experimental resolution of a few keV and that  $J > 1/2$ . After these two early total cross section measurements, no new measurements were made until those of Harvey *et al.* [10] in 1992. That measurement obtained significantly improved energy resolution and uncertainty giving  $E_n = 433.35(3)$  keV,  $\Gamma_n = 2.46(4)$  keV,  $\Gamma_\gamma = 40(70)$  eV and  $J = 7/2$ . In particular, their significantly improved energy resolution resulted in the first firm spin assignment for this resonance, as the resonance height is indicative of the spin of the corresponding level.

Although it is a small effect, the peak cross section produced by a  $7/2^+$  resonance in the  $R$ -matrix fit slightly overshoots the two highest data points of Harvey *et al.*

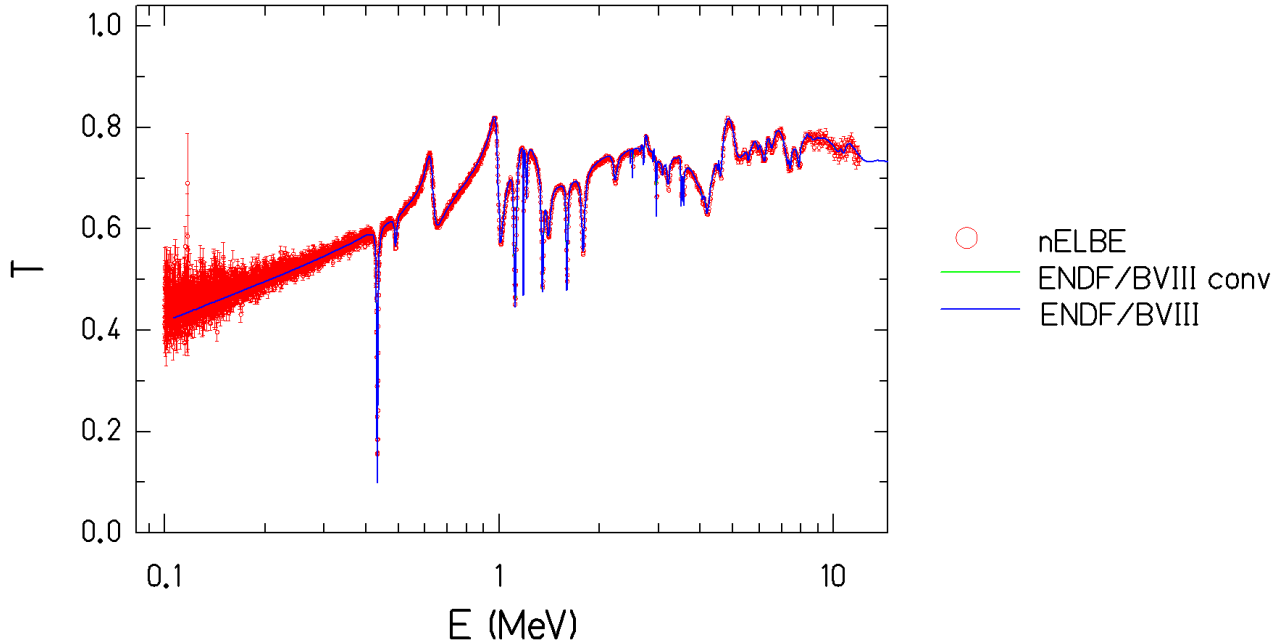


FIG. 9. The measured neutron transmission of nitrogen with an areal density of 0.19736(24) atoms/barn in the full energy range of 0.1 to 12 MeV. The time-of-flight bin size is 0.488 ns. The experimental data are compared with calculated transmission from ENDF-B/VIII.0 point wise total cross sections (blue) and a transmission curve including the experimental resolution function (green).

[10]. To resolve this disagreement, Harvey *et al.* [10] included a  $\gamma$ -ray partial width of 40(70) eV to damp the height of the resonance. It seems likely that the quoted value of this width is a typographical error and should be 70(40) eV. Indeed, including the larger value of 70 eV for  $\Gamma_\gamma$  does exactly reproduce their experimental data. However, there is no experimental evidence for such a strong  $\gamma$ -ray decay from this state. Conversely, the  $R$ -matrix fit undershoots the highest cross section points in the present data. These inconsistencies emphasize the small statistical uncertainties achieved for the present measurements and those of Harvey *et al.* [10] and the strong sensitivity to experimental resolution for this narrow resonance.

Unlike most of the higher energy resonances observed in  $^{14}\text{N}+n$ , the one at  $E_n = 433$  keV has very small decay branches to both the proton or  $\alpha$ -particle channels, which hinders its experimental accessibility using other types of reactions. Wang *et al.* [21] was able to observe the corresponding resonance using the  $^{14}\text{C}(p,n)^{14}\text{N}$  reaction ( $E_n = 434(1)$  keV,  $\Gamma = 2.4(5)$  keV,  $\Gamma_p = 9.0(15)$  meV), confirming a very weak proton decay branch. Finally, the very recent low-energy measurement of the  $^{11}\text{B}(\alpha,n)^{14}\text{N}$  reaction by Borgwardt *et al.* [47] observed the corresponding resonance in that reaction for the first time and found  $\Gamma_\alpha = 315(48)$  neV. Note that these partial widths did assume that the corresponding state had

$$J = 7/2.$$

Fig. 13 shows a comparison between the measurement of the 433 keV resonance from this work and that of Harvey *et al.* [10]. In this work, the resonance has been observed with a smaller peak cross section and a somewhat larger width. The best fit is obtained with a spin-parity of  $J = 5/2^+$ , with  $E_n = 433.15(1)$  keV,  $\Gamma_n = 2.82(2)$  keV and  $\Gamma_\alpha = 438(57)$  neV.  $\Gamma_p$  was fixed to the value of 9.0(15) meV as reported by Wang *et al.* [21] and this small partial width was found to not influence the shape of the total capture cross section compared to the present uncertainties. The larger total width may seem to be an indication of an uncorrected resolution effect, but this does not seem to be the case as the nELBE resolution function has a small effect on the resonance shape at these energies. Further, the shape of the resonance is very clearly Lorentzian, and the quality of the fit worsens considerably if it is convoluted with a Gaussian function.

On the data analysis side, a constant random background is subtracted in the time-of-flight spectra, see Eq. (1). A possible beam-related correlated background is difficult to determine in the fast neutron range, as this would require the use of “black resonances” in the energy range of several hundred keV neutron energy [53, 54] to determine background levels for both target in/out measurements. From other transmission measurements using a 90 mm thick  $^{nat}\text{Fe}$  sample at nELBE [55], the

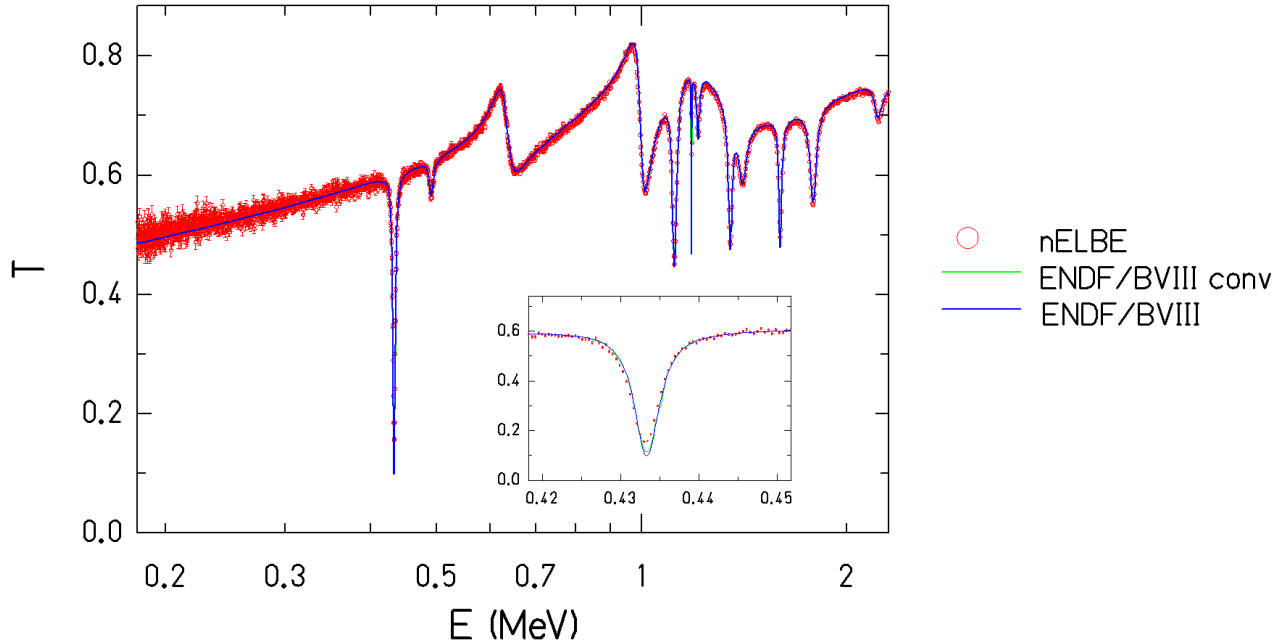


FIG. 10. The measured neutron transmission of nitrogen in the energy range below 2 MeV, description of data as in Fig. 9. The experimental resolution is sufficient to resolve most known resonances with the exception of the resonance at 1184 keV, which has a total width of 1.4 keV. The inset shows the resonance at 433 keV. The calculated transmission based on ENDF/B VIII is too small at the resonance peak.

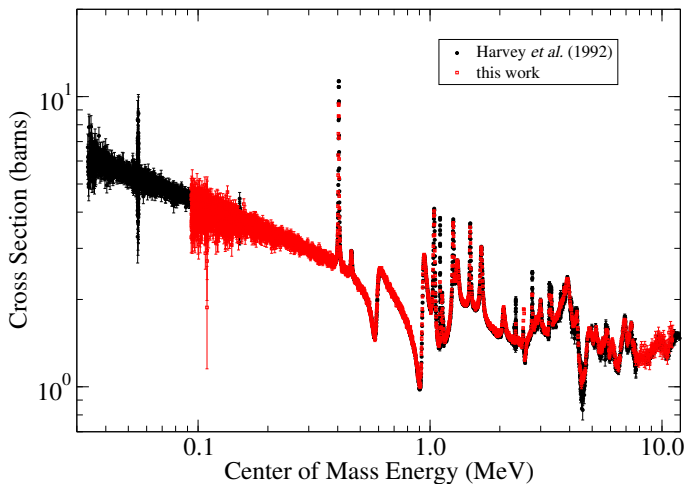


FIG. 11. Comparison of the  $^{14}\text{N}$  total cross section data of this work with that of Harvey *et al.* [10]. The data sets are largely consistent when experimental resolution is applied.

beam correlated background in resonances from 100 to 500 keV was estimated because at these resonance peaks the experimental transmission factor is determined to be 0.005 or lower. It was estimated that the beam correlated background at this energy is a factor of 2.5 higher than the uncorrelated constant background at time-of-

flight longer than  $4.5 \mu\text{s}$ . A straightforward subtraction of a background level that is a factor 2.5 higher than the constant background observed in the nitrogen transmission measurement both for target in/out measurements leads to a smaller transmission factor at the resonance peak (433 keV) by a factor 0.974. This corresponds to a possible higher peak cross section of 1.3%. The observed transmission of Harvey *et al.* [10] at 433 keV can be estimated to be 0.0143, which is a factor of 10 smaller than in this work (0.1557). This tends to make the observed peak value in the experiment of Harvey *et al.* more sensitive to the background subtraction.

One additional complication is that there is some ambiguity in the  $R$ -matrix fitting of the non-resonant portion of the total neutron cross section because it is produced by some unknown number of subthreshold resonances. This allows for flexibility in the absolute total cross section resulting from the  $R$ -matrix fit and the experimental data also has some uncertainty in its absolute scale, which is estimated to be 1% for the present measurements (see Sec. III) and perhaps as small as 0.5% for the data of Harvey *et al.* [10]. If normalization factors for the data sets are allowed to vary in the fits, this does result in an improvement in the fitting of the data. For instance, for the data of Harvey *et al.* [10], an increase in the reported cross sections of 1.8% makes it possible to fit the highest cross section data points at the peak of the



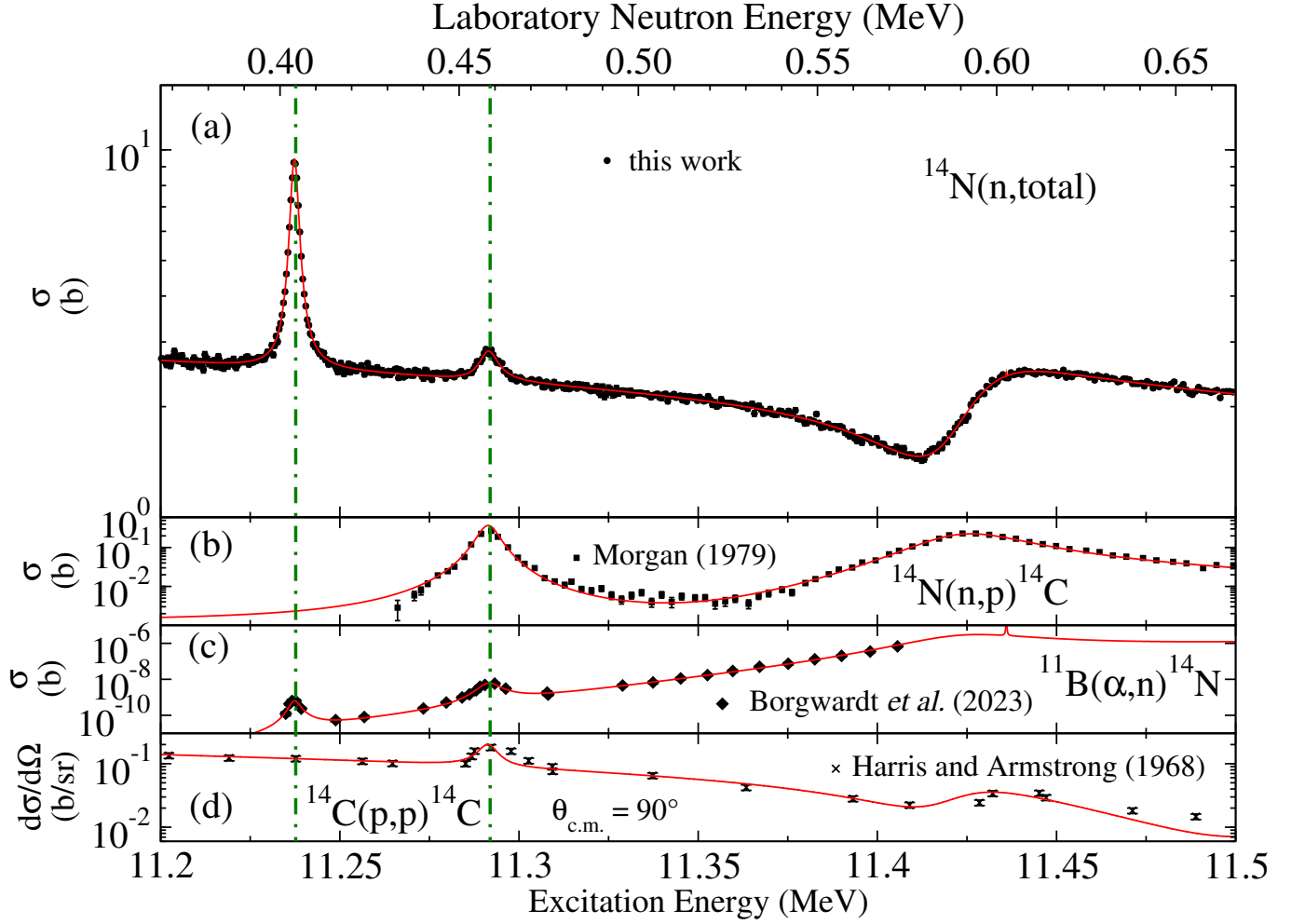


FIG. 12. Multichannel  $R$ -matrix fit (solid red line) that includes (a) the present total neutron cross section data, (b) the  $^{14}\text{N}(n,p)^{14}\text{C}$  data of Morgan [6], (c) the  $^{11}\text{B}(\alpha,n)^{14}\text{N}$  data of Borgwardt *et al.* [47] and (d) the  $^{14}\text{C}(p,p)^{14}\text{C}$  data of Harris and Armstrong [26].

433 keV resonance, without any significant  $\gamma$ -ray width. Likewise, if the scale of the present data are reduced by 5%, the fit is able to match the highest cross section data in the present measurements.

## VI. SUMMARY

New measurements of the  $^{14}\text{N}+n$  total cross section have been performed at the nELBE facility at HZDR. In particular, the measurement was undertaken in order to cross-check the data reported by Harvey *et al.* [10], which have a high sensitivity and energy resolution, but they lack detailed information regarding the experimental conditions. Except for the lowest energy resonance at  $E_n = 433$  keV, the present measurements are found to be in good agreement with those reported by Harvey *et al.* [10], giving improved confidence in the present ENDF/B evaluation, which is based largely on the measurements of Harvey *et al.* [10]. Further, a smaller cross section has

been found for the lowest energy resonance that implies a spin-parity assignment of  $5/2$ , rather than the value of  $7/2$  assigned previously.

Because of the unparalleled sensitivity of total neutron cross sections, they provide a great deal of constraint for  $R$ -matrix fits that are used to evaluate resolved resonance regions. Therefore, the improved understanding and confidence in the accuracy of the  $^{14}\text{N}+n$  total cross section of the present data and those of Harvey *et al.* [10] will provide improved future evaluations for not only the  $^{14}\text{N}+n$  total cross section but also reaction cross sections like  $^{14}\text{N}(n,p)^{14}\text{C}$  and  $^{11}\text{B}(\alpha,n)^{14}\text{N}$ .

## ACKNOWLEDGMENTS

This research utilized resources from the Notre Dame Center for Research Computing and was supported by the National Science Foundation through Grant No. PHY-2310059 (University of Notre Dame Nuclear Science

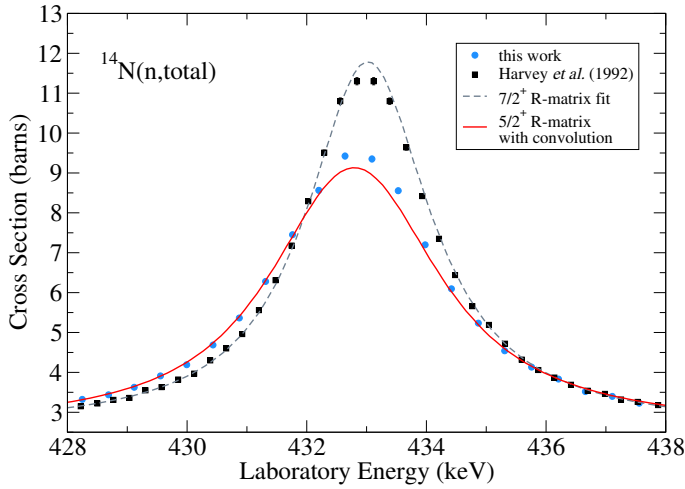


FIG. 13. Comparison of the data of this work to that of Harvey *et al.* [10]. The data of Harvey *et al.* [10] is described well by a  $R$ -matrix calculation using a level of  $J^\pi = 7/2^+$ , while that of the present work requires a lower spin of  $J^\pi = 5/2^+$ .

Laboratory), the Joint Institute for Nuclear Astrophysics through Grant No. PHY-1430152 (JINA Center for the Evolution of the Elements). A.R.J. acknowledges funding from the Euratom research and training programme 2014-2018 under grant agreement No 847594 (ARIEL). Parts of this research were carried out at ELBE at the Helmholtz-Zentrum Dresden - Rossendorf e. V., a member of the Helmholtz Association.

- 
- [1] A. Wallner, M. Bichler, K. Buczak, I. Dillmann, F. Käppeler, A. Karakas, C. Lederer, M. Lugaro, K. Mair, A. Mengoni, G. Schätzle, P. Steier, and H. P. Trautvetter, *Phys. Rev. C* **93**, 045803 (2016).
  - [2] P. E. Koehler and H. A. O'Brien, *Phys. Rev. C* **39**, 1655 (1989).
  - [3] K. Brehm, H. W. Becker, C. Rolfs, H. P. Trautvetter, F. Kappeler, and W. Ratynski, *Zeitschrift für Physik A Hadrons and Nuclei* **330**, 167 (1988).
  - [4] T. Sanami, M. Baba, I. Matsuyama, S. Matsuyama, T. Kiyosumi, Y. Nauchi, and N. Hirakawa, *Nuclear Instruments and Methods in Physics Research A* **394**, 368 (1997).
  - [5] T. Shima, K. Watanabe, T. Irie, H. Sato, and Y. Nagai, *Nuclear Instruments and Methods in Physics Research A* **356**, 347 (1995).
  - [6] G. L. Morgan, *Nuclear Science and Engineering* **70**, 163 (1979).
  - [7] C. H. Johnson and H. H. Barschall, *Physical Review* **80**, 818 (1950).
  - [8] P. Torres-Sánchez, J. Praena, I. Porras, M. Sabaté-Gilarte, C. Lederer-Woods, O. Aberle, V. Alcayne, S. Amaducci, J. Andrzejewski, L. Audouin, V. Bécaries, V. Babiano-Suarez, M. Bacak, M. Barbagallo, F. Bečvář, G. Bellia, E. Berthoumieux, J. Billowes, D. Bosnar, A. Brown, M. Busso, M. Caamaño, L. Caballero, F. Calviño, M. Calviani, D. Cano-Ott, A. Casanovas, F. Cerutti, Y. Chen, E. Chiaveri, N. Colonna, G. Cortés, M. Cortés-Giraldo, L. Cosentino, S. Cristallo, L.-A. Damone, M. Diakaki, M. Dietz, C. Domingo-Pardo, R. Dressler, E. Dupont, I. Durán, Z. El-eme, B. Fernández-Domínguez, A. Ferrari, F. J. Ferrer, P. Finocchiaro, V. Furman, K. Göbel, R. Garg, A. Gawlik-Ramiega, B. Geslot, S. Gilardoni, T. Glodariu, I. Gonçalves, E. González-Romero, C. Guerrero, F. Gunsing, H. Harada, S. Heinitz, J. Heyse, D. Jenkins, E. Jericha, F. Käppeler, Y. Kadi, A. Kimura, N. Kivel, M. Kokkoris, Y. Kopatch, M. Krčička, D. Kurtulgil, I. Ladarescu, H. Leeb, J. Lerendegui-Marco, S. L. Meo, S.-J. Lonsdale, D. Macina, A. Manna, T. Martínez, A. Masi, C. Massimi, P. Mastinu, M. Mastromarco, F. Matteucci, E.-A. Maugeri, A. Mazzone, E. Mendoza, A. Mengoni, V. Michalopoulou, P. M. Milazzo, F. Mingrone, A. Musumarra, A. Negret, R. Nolte, F. Ogállar, A. Oprea, N. Patronis, A. Pavlik, J. Perkowski, L. Persanti, J.-M. Quesada, D. Radeck, D. Ramos-Doval, T. Rauscher, R. Reifarth, D. Rochman, C. Rubbia, A. Saxena, P. Schillebeeckx, D. Schumann, G. Smith, N. Sosnin, A. Stamatopoulos, G. Tagliente, J. Tain, Z. Talip, A. Tarifeño-Saldivia, L. Tassan-Got, A. Tsinganis, J. Ulrich, S. Urlass, S. Valenta, G. Vannini, V. Variale, P. Vaz, A. Ventura, V. Vlachoudis, R. Vlastou, A. Wallner, P. Woods, T. Wright, P. Žugec, and n TOF Collaboration, *Phys. Rev. C* **107**, 064617 (2023), arXiv:2212.05128 [nucl-ex].
  - [9] A. J. M. Plompen, O. Cabellos, C. De Saint Jean, M. Fleming, A. Algara, M. Angelone, P. Archier, E. Bauge, O. Bersillon, A. Blokhin, F. Cantargi, A. Chebboubi, C. Diez, H. Duarte, E. Dupont, J. Dyrda, B. Erasmus, L. Fiorito, U. Fischer, D. Flammini, D. Foligno, M. R. Gilbert, J. R. Granada, W. Haeck, F.-J. Hambsch, P. Helgesson, S. Hilaire, I. Hill, M. Hursin, R. Ichou, R. Jacquemin, B. Jansky, C. Jouanne, M. A. Kellett, D. H. Kim, H. I. Kim, I. Kodeli, A. J. Koning, A. Y. Konobeyev, S. Kopecky, B. Kos, A. Krása, L. C. Leal, N. Leclaire, P. Leconte, Y. O. Lee, H. Leeb, O. Litaize, M. Majerle, J. I. Márquez Damián, F. Michel-Sendis, R. W. Mills, B. Morillon, G. Noguère, M. Pecchia, S. Pelloni, P. Pereslavtsev, R. J. Perry, D. Rochman, A. Röhrmoser, P. Romain, P. Romojaro, D. Roubtsov, P. Sauvan, P. Schillebeeckx, K. H. Schmidt, O. Serot, S. Simakov, I. Sirakov, H. Sjöstrand, A. Stankovskiy, J. C. Sublet, P. Tamagno, A. Trkov, S. van der Marck, F. Álvarez Velarde, R. Villari, T. C. Ware, K. Yokoyama,

- and G. Žerovnik, *The European Physical Journal A* **56**, 10.1140/epja/s10050-020-00141-9 (2020).
- [10] J. A. Harvey, N. W. Hill, N. M. Larson, and D. C. Larson, in *Nuclear Data for Science and Technology. Series: Research Reports in Physics* (Springer Berlin Heidelberg (Berlin, Heidelberg), 1992) pp. 729–731.
  - [11] V. McLane and Members of the Cross Section Evaluation Working Group, *ENDF-201, ENDF/B-VI Summary Documentation, Supplement I, ENDF/HE-VI Summary Documentation*, Tech. Rep. (National Nuclear Data Center, Brookhaven National Laboratory, Upton, New York 11973-5000, 1996).
  - [12] G. M. Hale, P. G. Young, M. Chadwick, and Z. P. Chen, in *Nuclear Data for Science and Technology. Series: Research Reports in Physics* (Springer Berlin Heidelberg (Berlin, Heidelberg), 1992) pp. 921–923.
  - [13] D. A. Brown, M. B. Chadwick, R. Capote, A. C. Kahler, A. Trkov, M. W. Herman, A. A. Sonzogni, Y. Danon, A. D. Carlson, M. Dunn, D. L. Smith, G. M. Hale, G. Arbanas, R. Arcilla, C. R. Bates, B. Beck, B. Becker, F. Brown, R. J. Casperson, J. Conlin, D. E. Cullen, M. A. Descalle, R. Firestone, T. Gaines, K. H. Guber, A. I. Hawari, J. Holmes, T. D. Johnson, T. Kawano, B. C. Kiedrowski, A. J. Koning, S. Kopecky, L. Leal, J. P. Lestone, C. Lubitz, J. I. Márquez Damián, C. M. Mattoon, E. A. McCutchan, S. Mughabghab, P. Navratil, D. Neudecker, G. P. A. Nobre, G. Noguere, M. Paris, M. T. Pigni, A. J. Plompen, B. Pritychenko, V. G. Pronyaev, D. Roubtsov, D. Rochman, P. Romano, P. Schillebeeckx, S. Simakov, M. Sin, I. Sirakov, B. Sleaford, V. Sobes, E. S. Soukhovitskii, I. Stetcu, P. Talou, I. Thompson, S. van der Marck, L. Welsch-Sherill, D. Wiarda, M. White, J. L. Wormald, R. Q. Wright, M. Zerkle, G. Žerovnik, and Y. Zhu, *Nuclear Data Sheets* **148**, 1 (2018).
  - [14] R. J. deBoer and P. Dimitriou, *International Nuclear Data Evaluation Network (INDEN) Meeting on the Evaluation of Light Elements*, Tech. Rep. INDC(NDS)-0768 (International Atomic Energy Agency, Vienna, Austria, 2018).
  - [15] R. J. deBoer and P. Dimitriou, *International Nuclear Data Evaluation Network (INDEN) on the Evaluation of Light Elements (2)*, Tech. Rep. INDC(NDS)-0788 (International Atomic Energy Agency, Vienna, Austria, 2019).
  - [16] H. Leeb, R. J. deBoer, I. Thompson, and P. Dimitriou, *International Nuclear Data Evaluation Network (INDEN) on the Evaluation of Light Elements (3)*, Tech. Rep. INDC(NDS)-0827 (International Atomic Energy Agency, Vienna, Austria, 2021).
  - [17] P. J. Reimer, T. A. Brown, and R. W. Reimer, *Radio-carbon* **46**, 1299 (2004).
  - [18] G. S. Burr, Bomb carbon, in *Encyclopedia of Scientific Dating Methods*, edited by W. J. Rink and J. Thompson (Springer Netherlands, Dordrecht, 2021) pp. 1–1.
  - [19] M. Niecke, M. Niemeier, R. Weigel, and H. Wirzba-Lorenz, *Nucl. Phys. A* **289**, 408 (1977).
  - [20] L. Van Der Zwan and K. W. Geiger, *Nucl. Phys. A* **246**, 93 (1975).
  - [21] T. R. Wang, R. B. Vogelaar, and R. W. Kavanagh, *Phys. Rev. C* **43**, 883 (1991).
  - [22] R. A. Dayras, Z. E. Switkowski, and T. A. Tombrello, *Nucl. Phys. A* **261**, 365 (1976).
  - [23] A. Turowiecki, A. Saganek, M. Siemiński, E. Wesołowski, and Z. Wilhelmi, *Nucl. Phys. A* **468**, 29 (1987).
  - [24] L. C. McIntyre, J. A. Leavitt, M. D. Ashbaugh, Z. Lin, and J. O. Stoner, *Nuclear Instruments and Methods in Physics Research B* **64**, 457 (1992).
  - [25] J. R. Liu, Z. S. Zheng, and W. K. Chu, *Nuclear Instruments and Methods in Physics Research B* **108**, 1 (1996).
  - [26] W. R. Harris and J. C. Armstrong, *Physical Review* **171**, 1230 (1968).
  - [27] J. D. Henderson, E. L. Hudspeth, and W. R. Smith, *Physical Review* **172**, 1058 (1968).
  - [28] F. C. Young, A. S. Figuera, and C. E. Steerman, *Nucl. Phys. A* **173**, 239 (1971).
  - [29] W. D. Roseborough, J. J. McCue, W. M. Preston, and C. Goodman, *Physical Review* **83**, 1133 (1951).
  - [30] R. M. Sanders, *Physical Review* **104**, 1434 (1956).
  - [31] J. H. Gibbons and R. L. Macklin, *Physical Review* **114**, 571 (1959).
  - [32] G. A. Bartholomew, F. Brown, H. E. Gove, A. E. Litherland, and E. B. Paul, *Canadian Journal of Physics* **33**, 441 (1955).
  - [33] J. L. Fowler and C. H. Johnson, *Physical Review* **98**, 728 (1955).
  - [34] F. Gabbard, H. Bichsel, and T. W. Bonner, *Nuclear Physics* **14**, 277 (1959).
  - [35] J. J. Hinchey, P. H. Stelson, and W. M. Preston, *Physical Review* **86**, 483 (1952).
  - [36] C. H. Johnson, B. Petree, and R. K. Adair, *Physical Review* **84**, 775 (1951).
  - [37] J. Klug, E. Altstadt, C. Beckert, R. Beyer, H. Freiesleben, V. Galindo, E. Grosse, A. Junghans, D. Légrády, B. Naumann, K. Noack, G. Rusev, K. Schilling, R. Schlenk, S. Schneider, A. Wagner, and F.-P. Weiss, *Nuclear Instruments and Methods in Physics Research Section A: Accelerators, Spectrometers, Detectors and Associated Equipment* **577**, 641 (2007).
  - [38] R. Beyer, E. Birgersson, Z. Elekes, A. Ferrari, E. Grosse, R. Hannaske, A. Junghans, T. Kögler, R. Massarczyk, A. Matić, R. Nolte, R. Schwengner, and A. Wagner, *Nuclear Instruments and Methods in Physics Research Section A: Accelerators, Spectrometers, Detectors and Associated Equipment* **723**, 151 (2013).
  - [39] R. Beyer, E. Grosse, K. Heide, J. Hutsch, A. Junghans, J. Klug, D. Légrády, R. Nolte, S. Röttger, M. Sobiella, and A. Wagner, *Nuclear Instruments and Methods in Physics Research Section A: Accelerators, Spectrometers, Detectors and Associated Equipment* **575**, 449 (2007).
  - [40] S. Mughabghab, *Atlas of Neutron Resonances* (Elsevier, 2018).
  - [41] E. W. Lemmon, M. O. McLinden, and D. G. Friend, *Thermophysical Properties of Fluid Systems*, edited by P. Linstrom and W. Mallard, Vol. NIST Chemistry WebBook, NIST Standard Reference Database Number 69, (National Institute of Standards and Technology, Gaithersburg MD, 20899, 2016).
  - [42] Multi Branch System (MBS), [https://www.gsi.de/en/work/research/experiment\\_electronics/data\\_processing/data\\_acquisition/mbs](https://www.gsi.de/en/work/research/experiment_electronics/data_processing/data_acquisition/mbs), accessed: 2025-03-17.
  - [43] R. Beyer, A. R. Junghans, P. Schillebeeckx, I. Sirakov, T.-Y. Song, D. Bemmerer, R. Capote, A. Ferrari, A. Hartmann, R. Hannaske, J. Heyse, H. I. Kim, J. W. Kim, T. Kögler, C. W. Lee, Y.-O. Lee, R. Massarczyk, S. E. Müller, T. P. Reinhardt, M. Röder, K. Schmidt, R. Schwengner, T. Szücs, M. P. Takács, A. Wagner,

- L. Wagner, and S.-C. Yang, The European Physical Journal A **54**, 81 (2018).
- [44] R. Hannaske, Z. Elekes, R. Beyer, A. Junghans, D. Bemmerer, E. Birgersson, A. Ferrari, E. Grosse, M. Kempe, T. Kögler, M. Marta, R. Massarczyk, A. Matic, G. Schramm, R. Schwengner, and A. Wagner, The European Physical Journal A **49**, 137 (2013).
- [45] R. E. Azuma, E. Uberseder, E. C. Simpson, C. R. Brune, H. Costantini, R. J. de Boer, J. Görres, M. Heil, P. J. Leblanc, C. Ugalde, and M. Wiescher, Phys. Rev. C **81**, 045805 (2010).
- [46] R. J. deBoer, Q. Liu, Y. Chen, M. Couder, J. Görres, E. Lamere, A. M. Long, S. Lyons, K. Manukyan, L. Morales, D. Robertson, C. Seymour, G. Seymour, E. Stech, B. Vande Kolk, and M. Wiescher, in *Journal of Physics Conference Series*, Journal of Physics Conference Series, Vol. 1668 (2020) p. 012011.
- [47] T. C. Borgwardt, R. J. deBoer, A. Boeltzig, M. Couder, J. Görres, A. Gula, M. Hanhardt, K. V. Manukyan, T. Kadlecik, D. Robertson, F. Strieder, and M. Wiescher, Phys. Rev. C **108**, 035809 (2023).
- [48] C. R. Brune, Phys. Rev. C **66**, 044611 (2002), arXiv:nucl-th/0207048 [nucl-th].
- [49] A. M. Lane and R. G. Thomas, Reviews of Modern Physics **30**, 257 (1958).
- [50] D. Odell, C. R. Brune, D. R. Phillips, R. J. deBoer, and S. N. Paneru, Frontiers in Physics **10**, 888476 (2022), arXiv:2112.12838 [nucl-th].
- [51] D. Foreman-Mackey, D. W. Hogg, D. Lang, and J. Goodman, PASP **125**, 306 (2013), arXiv:1202.3665 [astro-ph.IM].
- [52] See Supplemental Material at [URL will be inserted by publisher] for additional details of the MCMC analysis.
- [53] P. Schillebeeckx, B. Becker, Y. Danon, K. Guber, H. Harada, J. Heyse, A. Junghans, S. Kopecky, C. Massimi, M. Moxon, N. Otuka, I. Sirakov, and K. Volev, Nuclear Data Sheets **113**, 3054 (2012).
- [54] D. Larson, N. Larson, J. Harvey, N. Hill, and C. Johnson, *ENDF-333, Application of New Techniques to ORELA Neutron Transmission Measurements and their Uncertainty Analysis: The Case of Natural Nickel from 2 keV to 20 MeV*, Tech. Rep. ORNL/TM-8203 (Oak Ridge National Laboratory, 1983).
- [55] A. Junghans, R. Beyer, R. Capote, D. Bemmerer, T. Hensel, T. Kögler, S. Müller, K. Römer, K. Schmidt, R. Schwengner, S. Turkat, J. Turko, and S. Urlaß, Annals of Nuclear Energy **218**, 111363 (2025).